Research Paper

Analysis of early stage osteonecrosis of the human femoral head and the mechanism of femoral head collapse

Cheng Wang[1,2], Haoye Meng[1], Yu Wang[1], Bin Zhao[1,4], Chenyang Zhao[6], Weijia Sun[3], Yun Zhu[1], Bingxing Han[3], Xueling Yuan[1], Ruoxi Liu[1], Xin Wang[5], Aiyuan Wang[1], Quanyi Guo[1], Jiang Peng[✉], Shibi Lu[1]

1. Institute of Orthopedics,Peking Key Lab of Regenerative Medicine in Orthopaedics, Key Lab of Chinese PLA, Chinese PLA General Hospital
2. Department of orthopedics. Peking University Third Hospital
3. State Key Laboratory of Space Medicine Fundamentals and Application, China Astronaut Research and Training Center
4. Department of Orthopedics, General Hospital of Chinese people's armed police force
5. Department of Orthopedics, Urumqi General Hospital of Lanzhou Military Command
6. College of Life Science, University of Chinese Academy of Sciences

✉ Corresponding author: Jiang Peng, Institute of Orthopedics, Chinese PLA General Hospital, FuXing Road 28#, HaiDian District, 100853, Beijing, China. E-mail: pengjiang301@126.com

Abstract

We explored the mechanism of early stage osteonecrotic femoral head collapse by analyzing and comparing different regions in human osteonecrotic femoral head samples. Eight osteonecrotic femoral heads (ARCO II–III) were obtained from patients undergoing total hip arthroplasty. Bone structure was observed and evaluated by micro-computed tomography (CT) scans and pathology. Osteoblast and osteoclast activities were detected by tartrate-resistant acid phosphatase, alkaline phosphatase, and immunofluorescent staining. Some trabeculae had microfractures in the subchondral bone and necrotic region, which had lower bone mineral density, as well as trabecular thickness and number, but greater osteoclast activity. A sclerotic band had already appeared in certain samples which had greater trabecular thickness and number, bone mineral density, and osteoblast activity. The appearance of the femoral head did not change significantly in the early stage of osteonecrosis of the femoral head. However, osteoblast and osteoclast activities had already changed in different regions of the osteonecrotic femoral head, which may lead to eventual collapse of the femoral head. Therefore, osteonecrosis of the femoral head must be treated during the early stage. In addition, osteoblast activity should be promoted and osteoclast activity inhibited as early as possible to prevent collapse of an osteonecrotic femoral head.

Key words: Early-stage osteonecrosis, femoral head, micro-CT, osteoblast, osteoclast

Introduction

Osteonecrosis of the femoral head (ONFH), also called avascular necrosis of the femoral head, is a series of pathological processes caused by blood supply disorders in part of the femoral head[1]. Moya-Angeler et al.[2] reported that the number of patients with ONFH is increasing by 200,000–300,000 annually, and that the number of cumulative cases has attained 5–7.5 million in the United States. At the same time, the age of onset tends be earlier. A study by Harvard Medical School showed that the younger the patient, the more easily it is to have total hip replacement overhauling surgery [3]. In addition, the high incidence of osteonecrosis of the femoral head is a heavy social and family burden. Therefore, intervention is particularly important before collapse of a necrotic femoral head.

The most common etiology of ONFH is use of corticosteroids (51%), followed by use of alcohol (31%) [4-6]. About 5–25% of patients will be attacked by this disease if patients continually use

corticosteroids for more than 1 month. Risk increases with the quantity and duration of use. Other possible causes include scuba diving or high-pressure disease, systemic lupus erythematosus and other connective tissue diseases, autoimmune diseases, hyperlipidemia, fat embolism syndrome, and metabolic bone diseases[7]. However, about 15% of patients exhibit no obvious cause, and thus have what is termed idiopathic osteonecrosis of the femoral head. The best time to treat ONFH is at the early stage; a variety of treatments are available before collapse of an osteonecrotic femoral head. However, obvious limitations appear once the head collapses [8-11]. No method has been demonstrated to effectively stop progression of the disease before the femoral head collapses or to postpone progression of osteoarthritis after the femoral head has collapsed. In our previous study, we found that the distribution of osteoblastic and osteoclastic activities differs in the different regions of patients with late stage ONFH. In this study, we used the same method to conduct a detailed analysis of early stage osteonecrotic femoral head specimens. We validated our hypothesis by observing changes in bone microstructure and osteoblast and osteoclast activities, and explored the mechanism of femoral head collapse. We also discuss an effective method to prevent femoral head collapse.

Materials and Methods

Specimens Collected

Eight osteonecrotic femoral heads were collected from patients in the early stages of ONFH(ARCO grades II–III). The etiologies were trauma, alcohol, and hormonal. This study was performed in accordance with our approved institutional guidelines, and the protocol was reviewed and approved the by Ethical Committee of the Chinese People's Liberation Army General Hospital (No. 20150101). Informed consent was obtained from all patients.

Micro-computed tomography (CT) detection, evaluation, and bone histomorphometric analysis

The coronal plane of the femoral head was placed parallel to the examination bed in the test chamber of a micro-CT set with the following parameters: the reconstructed voxel size, 45 μm; scanning voltage, 80 kV; and scanning electric current, 450 mA. The samples were divided into subchondral bone, necrotic, sclerotic, and healthy regions, depending on the bone density of the image (Figure 1B). Three-dimensional (3D) regions of interest were selected in four regions (Figure 1C). Bone

metrological analysis and 3D reconstruction were performed using GE Microview (GE Medical, Milwaukee, WI, USA). We computed the following bone mineral parameters: bone mineral density (BMD), trabecular thickness (Tb.Th), trabecular separation (Tb.Sp), and trabecular number (Tb,N).

Specimen Preparation

After the micro-CT scan, all eight samples were cut into three parts along the coronal plane (Figure 1 A). Part I was used to prepare non-decalcified bone tissue pathological sections, part II was used for molecular biology detection, and part III was used to prepare paraffin pathological sections. Parts I and III were fixed in paraformaldehyde prior to pathological analysis and part II was stored at -80°C prior to quantitative real-time polymerase chain reaction (PCR).

Pathological Detection

Part I was used for non-decalcified bone tissue pathological sections. After fixing the tissue in 4% paraformaldehyde for 1 week, part I was dehydrated through a graded alcohol series for 4 weeks and immersed in xylene for 1 week. Part I was then embedded with polymethyl methacrylate under negative pressure. After solidification, the tissue was cut into 100-μm -thick slices with a hard-tissue slicing machine (Isomet 5000; BUEHLER, Dusseldorf, Germany). The slices were ground with 400-, 600-, 800-, and 1,200-grit sandpaper, polished with aluminum powder (0.05 mm), stained, and observed.

Part III was used to prepare paraffin-embedded pathological sections. After fixing the tissues in 4% paraformaldehyde for 1 week and clearing in phosphate-buffered saline (PBS), the samples were decalcified with 10% EDTA for 4 weeks, cut into 4 regions (subchondral bone, necrotic, sclerotic, and healthy regions), and dehydrated with an Automatic Tissue Dehydrator (Leica ASP200S). The samples were embedded in paraffin, cut into 5-μm-thick sections, stained with hematoxylin and eosin (HE), and observed.

Immunofluorescent Staining

Paraffin sections were baked in a 60°C oven for 30 min, dewaxed according to conventional procedures, immersed in distilled water for 2 min, and rinsed twice in PBS for 5 min each. After immersion in 3% H2O2 for 5–20 min, the sections were rinsed three times in PBS. Antigen retrieval was performed with 0.1 M citrate buffer solution (pH 6). The solution was boiled for 10 min and then cooled to room temperature. The sections were placed in a moist chamber, after which, anti-receptor activator of nuclear factor-κB ligand (RANKL), receptor activator

of nuclear factor-κB (RANK), osteoprotegerin (OPG), and bone morphogenetic protein-2 (BMP2) antibodies were added, and the sections were placed at 4°C overnight. The primary antibodies were discarded the next day and the sections washed three times for 5 min each with PBS. The secondary antibody was then added, and the samples were protected from light at room temperature for 15–30 min. After washing three times in PBS for 5 min each, glycerin was added, coverslips were added, and the sections were observed under a fluorescent microscope.
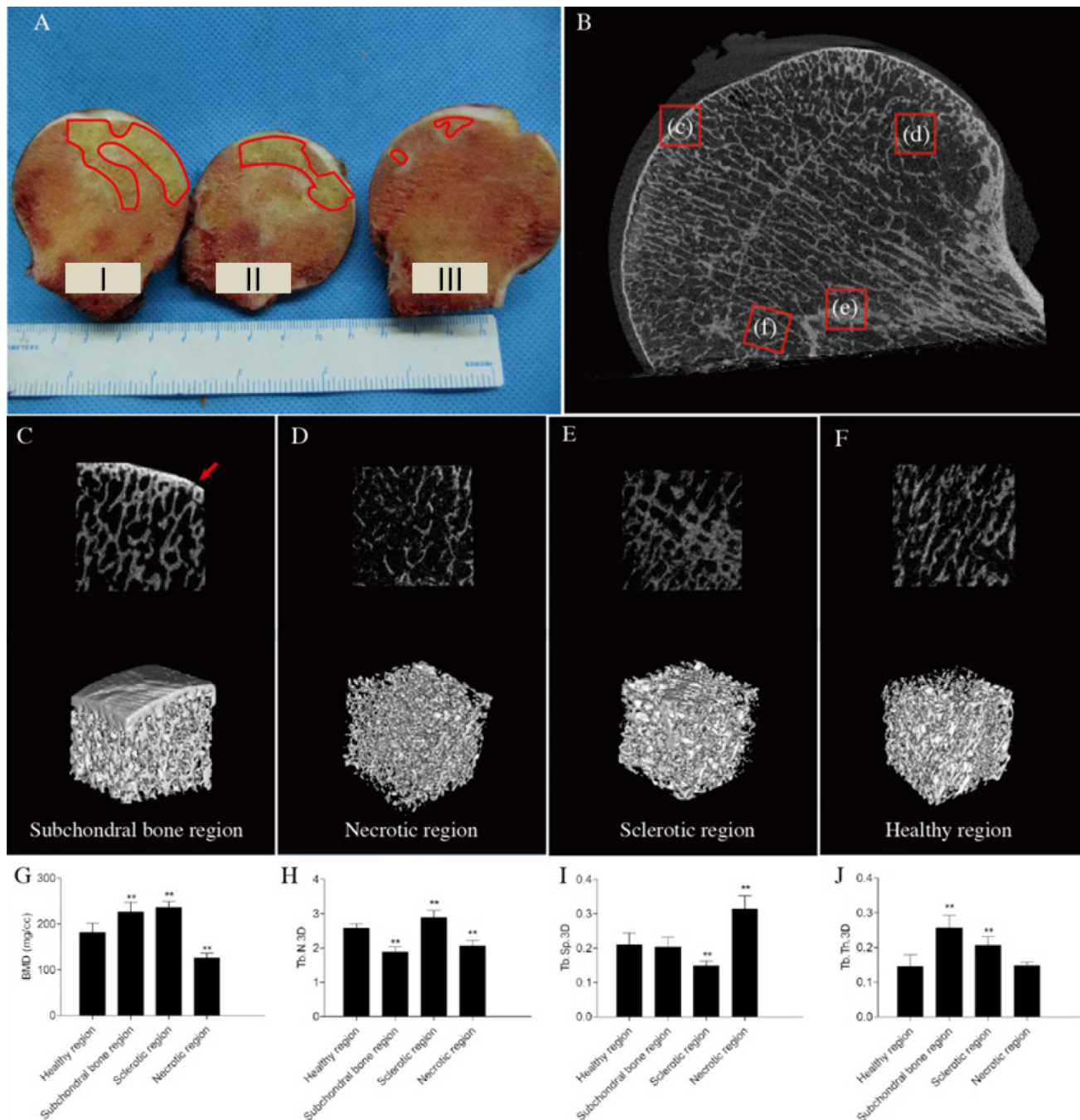

Figure 1. Structural analysis of early stage femoral head. osteonecrosis (A) Gross appearance of the femoral head. Although the femoral head does not collapse during the early stage of osteonecrosis, a clear necrotic area could be found in the femoral head (red line). Parts I, II, and III were used to make non-decalcified bone tissue pathological sections, detect molecular biology markers, and prepare paraffinized pathological sections, respectively. (B) Micro-computed tomography images (red arrows: microfractures). (C, D, E, and F) Two-dimensional reconstruction and three-dimensional (3D)-rendered images of different regions. (C) Subchondral bone region (red arrow: microfracture). (D) Necrotic region. (E) Sclerotic region. (F) Healthy region. (G–J) Bone histomorphometric data. (G) Bone mineral density (BMD). (H) Trabecular number 3D (Tb.N.3D). (I) Trabecular separation 3D (Tb.Sp.3D) (J) Trabecular thickness 3D (Tb.Th.3D). n = 8 for each group. All data are means ± SDs of those of three independent experiments. **$P < 0.05$ compared with the healthy region.

Tartrate-resistant Acid Phosphatase (TRAP) and Alkaline Phosphatase (ALP) staining

The paraffinized pathological sections were dewaxed in xylene and a graded ethanol series. TRAP staining was performed using a kit according to the manufacturer's instructions (387A-1KT; Sigma-Aldrich, St. Louis, MO, USA). ALP staining was performed using a kit according to the manufacturer's instructions (86R-1KT; Sigma-Aldrich, St. Louis, MO, USA). Osteoclast and osteoblast numbers were quantitated in the four different regions, and expressed as cells/mm2. Values were calculated for five nonconsecutive sections per region. Images were obtained with the aid of an Olympus BX51 microscope equipped with a DP71 camera (Olympus, Tokyo, Japan).

Quantitative Real-Time Polymerase Chain Reaction (PCR)

Bone tissues were cut from four different regions of part II of the femoral heads and ground into bone meal in liquid nitrogen. TRIzol was added to extract RNA from the bone meal. Primers were selected for RANK, RANKL, OPG, and BMP2 (Parkson, Beijing, China), and 1 µg RNA was added to a 20 µL volume reverse transcription system. cDNA was prepared by reverse transcription, and real-time PCR analysis was performed.

Western Blot

Bone tissues of different regions of the femoral head were pulverized in liquid nitrogen. Two milligrams of protein were added to RIPA lysis buffer, and the mixture was intermittently homogenized for 3 min in an ice bath. After sonication for 15 s and a 30-min incubation in the ice bath, the mixture was centrifuged at 12,000 x g for 30 min at 4°C. The supernatant was freeze-dried for 24 h and the protein precipitate diluted with 100 µL PBS containing protease inhibitors. After quantifying the protein amount and performing electrophoresis, the proteins were transferred onto polyvinylidene fluoride membranes. The membranes were probed with antibodies specific to OPG, RANK, RANKL, and BMP2 (Abcam, Cambridge, UK). Human GAPDH was used as a quantification marker. Signals were detected using secondary horseradish peroxidase-conjugated anti-mouse IgG and anti-rabbit IgG antibodies, and the membranes were immersed in enhanced chemiluminescent detection solution. The protein bands were quantified using an Epson GT-8000 laser scanner. The ratios of the protein band intensities relative to those of GAPDH were calculated for each sample.

Statistical Analysis

SPSS ver. 17.0 software (SPSS Inc., Chicago, IL, USA) was used for data analysis. All data are presented as the mean ± standard deviation. Groups were compared using single-factor analysis of variance (ANOVA). Pairs of groups were compared using the least significant difference test. A p-value < 0.05 was considered significant.

Results

Micro-CT images and results of bone histomorphometry

The micro-CT images of early stage ONFH revealed that the subchondral bone region had small microfractures and that the structural continuity of the trabeculae had changed in the necrotic region(Figures 1–D). Sclerotic bands were also found (Figure 1E). However, the overall shape of the femoral head was intact, and none of the femoral heads had collapsed (Figures 1A, B).

The bone histomorphometric parameters in other regions of trabecular bone were significantly different compared with those in the healthy region. The bone mineral densities of the subchondral bone and sclerotic regions increased, and those of necrotic regions decreased (Figure 1G). The number of trabeculae decreased significantly in the subchondral bone and necrotic regions compared to those in the healthy areas (Figure 1H). Trabecular separation was markedly greater in necrotic compared with healthy regions (Figure 1I). BMD and trabecular thickness increased significantly in the sclerotic region (Figures 1G, J).

Pathology results

HE staining of non-decalcified bone tissue pathological sections showed that the surface of the femoral head remained rounded and smooth, none of the femoral heads had collapsed. The subchondral bone structure remained intact. The extents of trabecular bone in necrotic regions were lower than those of sclerotic and normal regions. Obvious sclerotic bands were apparent in sclerotic regions, which had more bone trabeculae than other regions (Figure 2A). H&E staining of decalcified bone tissue sections showed that the subchondral and necrotic bone trabeculae contained many empty lacunae (Figures 2B, C). The trabecular thickness increased in the sclerotic region(Figure 2E). The trabeculae had better structural integrity and were regularly arranged in the healthy region, where normal bone cells and hematopoietic tissue were found (Figure 2D).
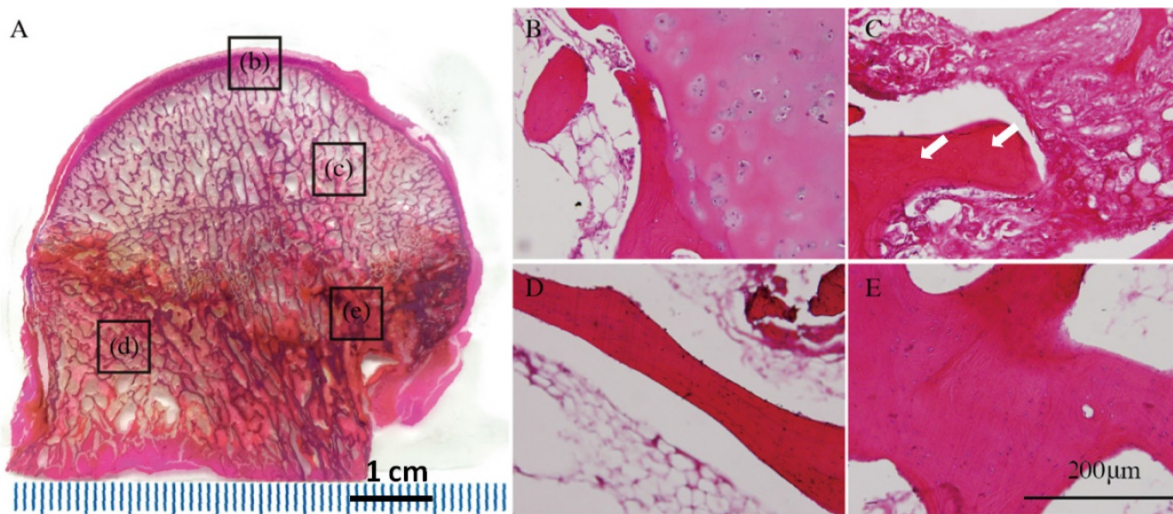
Figure 2. Results of the pathological sections of early stage osteonecrotic femoral heads. (A) Non-decalcified bone pathological sections. (B–E) Decalcified bone pathological sections. (B) Subchordal bone region. (C) Necrotic region. (D) Healthy region. (E) Sclerotic region. The white arrow in C indicates empty lacunae.
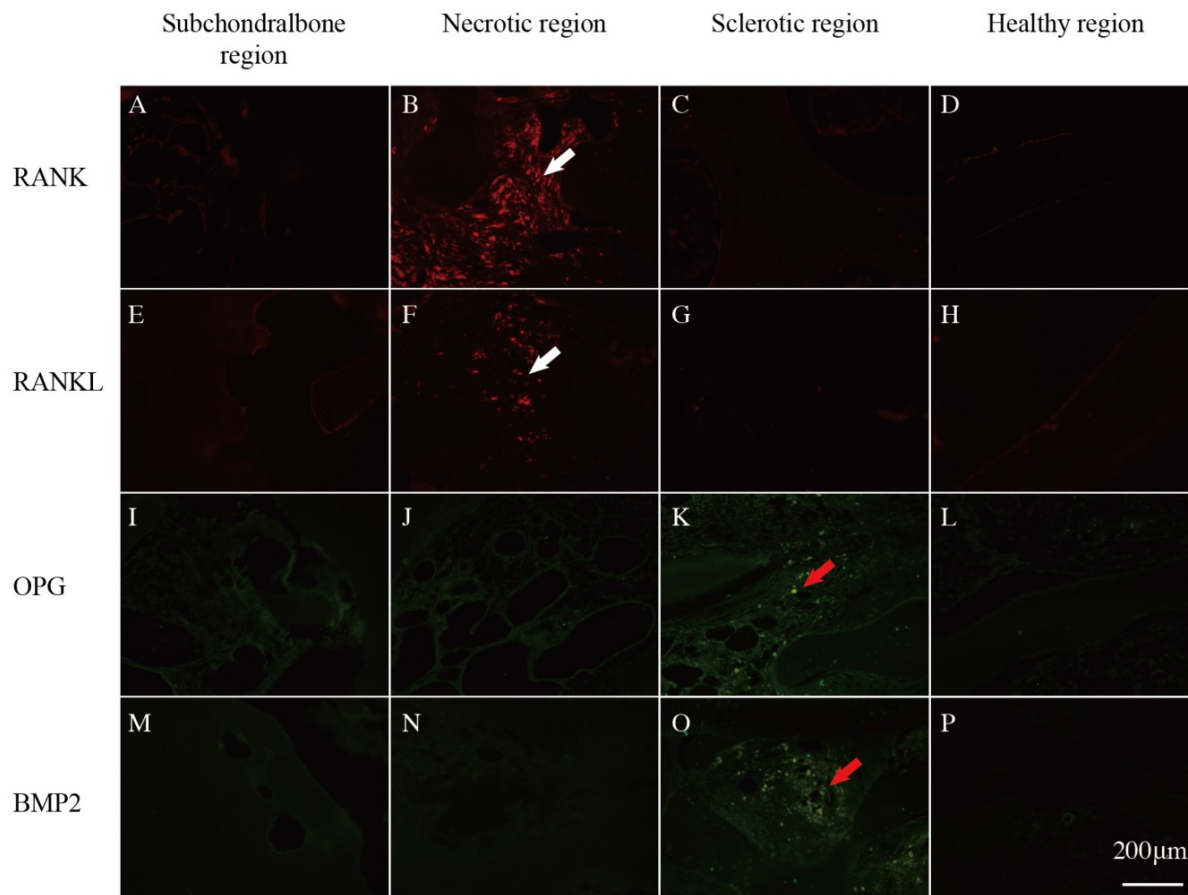

Figure 3. Immunofluorescent staining. (A–-D) Receptor activator of nuclear factor-κB (RANK), (E–H) receptor activator of nuclear factor-κB ligand (RANKL), (I–L) osteoprotegerin (OPG), and (M–P) bone morphogenetic protein-2 (BMP2) expression levels in different regions of early stage osteonecrotic femoral heads. (A, E, I, M) Subchordal bone region. (B, F, J, N) Necrotic region. (C, G, K, Q) Sclerotic region. (D, H, L, P) Healthy region. White arrows in B and F indicate the expression of RANK and RANKL. Red arrows in K and O indicate the expression of OPG and BMP2.

Immunofluorescent staining

RANK and RANKL were expressed in the subchordal bone and necrotic regions(Figures 3B, F), whereas OPG and BMP2 were expressed in the sclerotic region according to fluorescence microscopy (Figures 3K, Q).

Tartrate-resistant acid phosphatase (TRAP) and alkaline phosphatase (ALP) staining

TRAP and ALP staining was performed in the different regions of the ONFH. The results showed that the TRAP-positive cells were mainly distributed in the necrotic region (Figure 4A), where the osteoclasts had a crimson appearance and exhibited a multinuclear cellular structure (Figures 4B–E). ALP-positive cells were distributed principally in the sclerotic region, arranged around the trabecular bone, where the osteoblasts were dark brown in color (Figures 4F–I). Quantitatively, the number of osteoclasts increased in the necrotic region compared with that in the healthy regions and the number of osteoblasts increased in the sclerotic region (p < 0.05; Figures 4J, K).

Quantitative Real-time polymerase chain reaction (PCR)

BMP2 and OPG expression levels were increased in the sclerotic region of early stage ONFH compared with those in the healthy region (p < 0.05; Figures 5A, B). RANK and RANKL expression levels were increased in the necrotic region (p < 0.05; Figures 5C, D). The ratio of RANKL/OPG were increased in the subchondral bone and necrotic region (p < 0.05; Figure 5E).
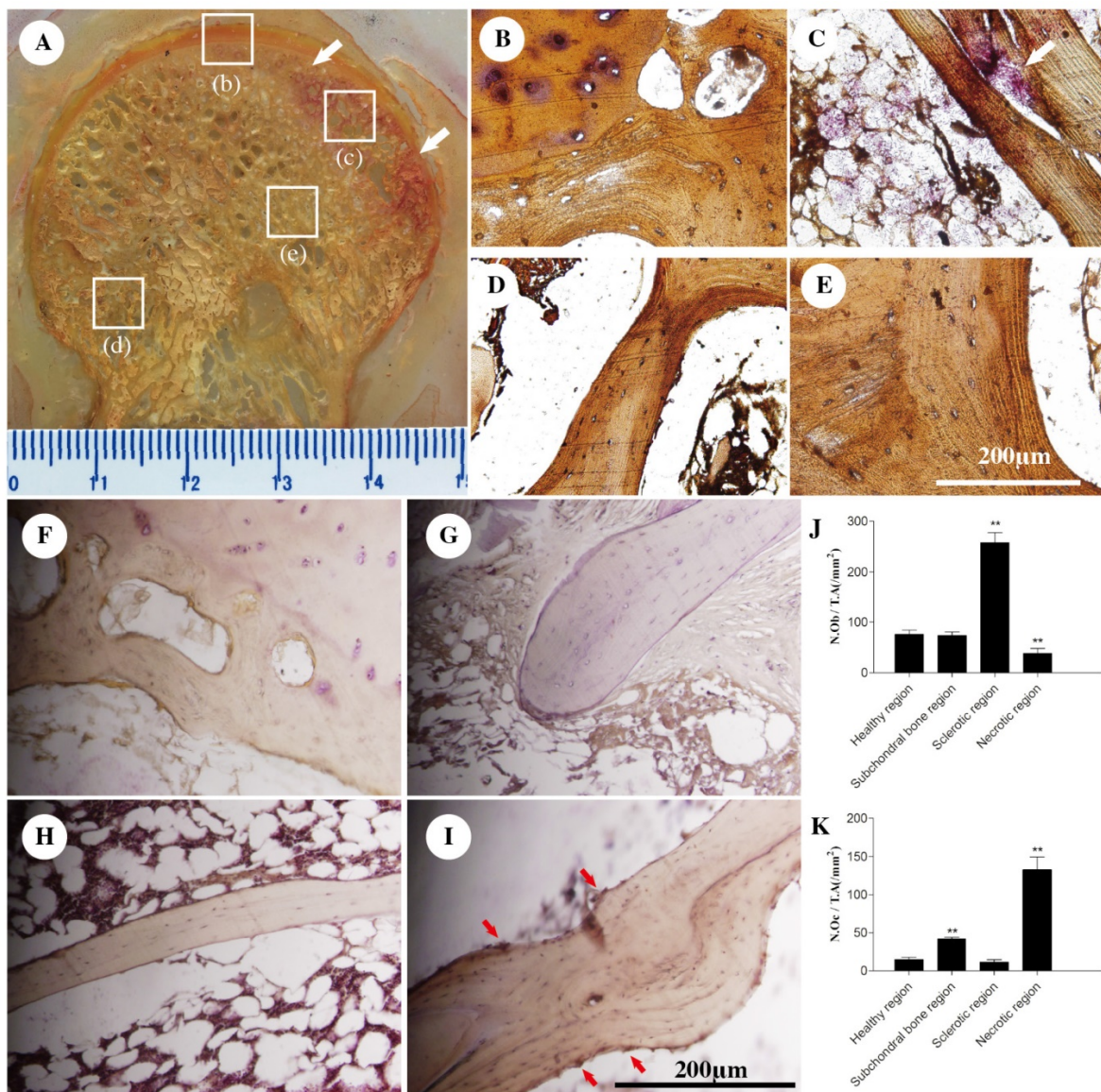

Figure 4. Tartrate-resistant acid phosphatase (TRAP) and alkaline phosphatase staining (ALP) staining. TRAP staining (A) Non-decalcified bone tissue pathological section. Paraffin sections. (B) Subchordral bone region. (C) Necrotic region. (D) Healthy region. (E) Sclerotic region. ALP staining (F) Subchordral bone region. (G) Necrotic region. (H) Healthy region. (I) Sclerotic region. (J, K) The numbers of osteoblasts and osteoclasts. N = 8 for each group. All data are the means ± SDs of those of three independent experiments. **P < 0.05 compared with the healthy region. White arrows in A and C indicate TRAP-positive regions. The red arrow in I indicates an ALP-positive region.
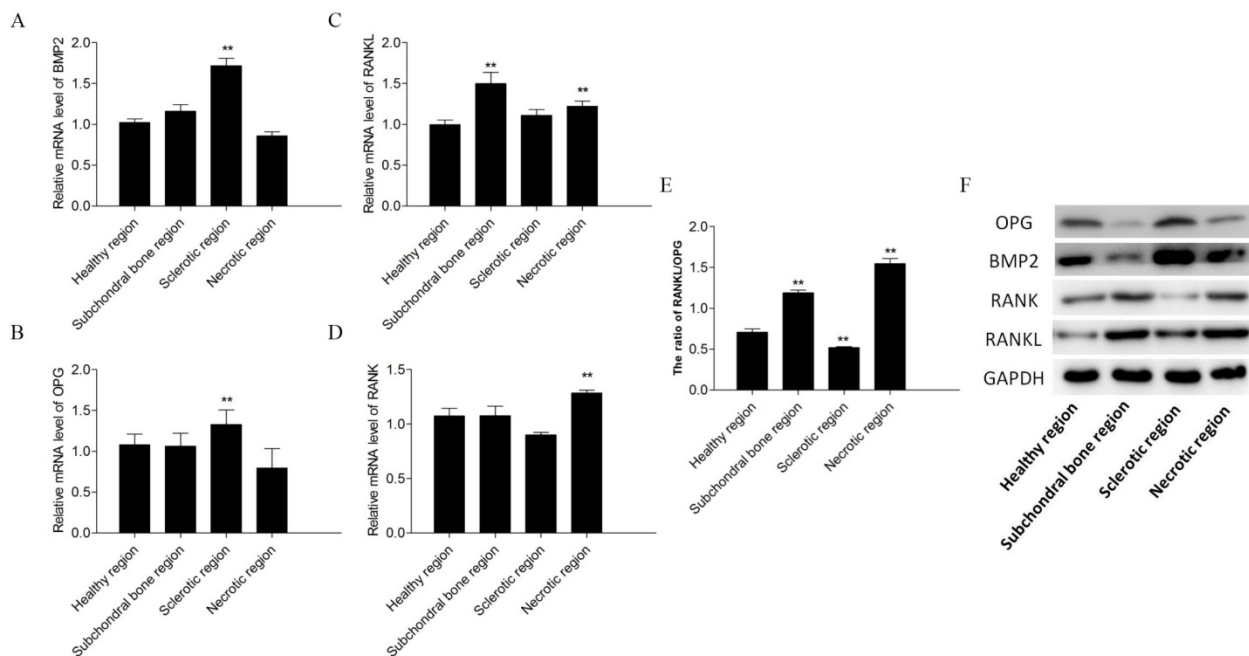
Figure 5. PCR and Western blot results. Relative mRNA levels of BMP2 (A), OPG (B), receptor activator of nuclear factor-κB ligand (RANKL) (C) and receptor activator of nuclear factor-κB (RANK) (D) in the subchondral bone, necrotic, sclerotic, and healthy regions. The ratio of RANKL/OPG(E). The expression levels of OPG, BMP2, RANK and RANKL in different regions of the osteonecrotic femoral head (F).

Western blot

OPG, RANK, RANKL, and BMP2 protein expression levels differed significantly in the different regions of early stage ONFH (Figure 5F). OPG and BMP2 levels were higher in the sclerotic region than in the healthy region, and RANK and RANKL expression levels were higher in the necrotic and subchondral bone regions compared to those in the healthy region.

Discussion

The human skeletal system maintains homeostasis and functional status through regulation of various cells, the most important of which are osteoblasts and osteoclasts. In addition, many orthopedic diseases are caused by changes in osteoblast and osteoclast functions, such as osteoporosis [12-14] and osteonecrosis[15, 16].

The OPG/RANKL/RANK signaling pathway is a very important mechanism that regulates bone metabolism [17]. OPG is a soluble RANKL decoy receptor that binds to three RANKL subtypes and blocks RANKL and RANK binding[18]. Gori et al. [19] found that developmental regulation of OPG and RANKL production contributes to the coordinated sequence of osteoclast and osteoblast differentiation during the bone remodeling cycle. In the present study, the expression of RANK and RANKL, which are bone resorption-related genes, increased per unit area in the necrotic and subchondral bone regions of

early stage ONFH. In addition, OPG and BMP2 expression levels were also increased in the sclerotic region, suggesting that osteoblast and osteoclast activities change significantly during the early stage of ONFH. In addition, the RANKL/OPG ratio per unit area increased in the necrotic and subchondral bone regions. Osteoclast activity was increased significantly in the necrotic region, whereas osteogenic activity increased significantly in the sclerotic region. In the process, micro-cavities appeared during bone reconstruction in the early stage of ONFH because of bone resorption overactivity, which also resulted in changes in the mechanical properties and structure of trabecular bone in the femoral head[20]. The cause of delayed or inadequate osteoblast-mediated bone formation activity and continuous load pressure and stress were concentrated in the damaged location[21, 22]. This eventually generates a large number of microfractures when the pressure is greater than the bone trabecula can withstand. New blood vessels often can only grow into the surrounding necrotic region, and new bone tissue appears around the necrotic region and forms a sclerotic band over time, which further prevents blood vessels from growing into the center of the necrotic area[23]. Thus, this area often cannot be effectively repaired and ultimately fractures, which collapses the femoral head.

Some researchers have reported that fracture and collapse of the ONFH is caused by a repeated load acting on bone that cannot be repaired in a timely

manner and multiple fatigue fractures develop in the femoral head. However, others do not believe this mechanism[24, 25]. In our previous study, we performed a series of tests and analyses on late stage ONFHs collected from patients and evaluated osteoblast and osteoclast activities in different regions of the femoral head [26]. The results showed that the bone trabecular microstructure changed significantly and that osteoblast and osteoclast activities were significantly different in different regions. Therefore, we speculated that collapse of the femoral head is strongly associated with changes in osteoblast and osteoclast activities. Osteoclast activity is stronger than osteogenic activity during repair of osteonecrosis and osteogenesis is less active than bone resorption. Due to continued load pressure, which results in repeated repair and repeated fractures, a repaired area appears between the necrotic and sclerotic regions. The emergence of a large number of fractures and cystic degeneration eventually leads to collapse of the femoral head.

We conducted a similar study here on early stage ONFH. Compared with the control group, the microstructure of the femoral head did not obviously change. The head shape remained round and only a small amount of bone absorption was evident inside the femoral head. However, the changes in osteoblast and osteoclast activities were similar to those evident at late stages of ONFH. The number of osteoclasts increased significantly per unit area in the necrotic region compared with that in the normal region, thereby leading to higher osteoclastic than osteogenic activity, which manifested as a destructive repair process. Normal bone repair mechanisms begin during osteoblast apoptosis, new blood vessels grow into the necrotic region, and sequestrum is absorbed along with the formation of new bone. Furthermore, we believe that a different repair process occurs in ONFH. Fan et al. [27] successfully established an emu ONFH collapse model, in which the extensive trabecular structure was rebuilt and the original trabecular bone was absorbed. This process is also called creeping substitution. That is to say, bone formation is slower than bone resorption during bone repair, which eventually leads to collapse of the femoral head; this has also been called "osteoclastic repair." The same author prepared another model by injecting anhydrous alcohol into the emu femoral head, but the head did not collapse. The original trabecular structure remained intact and new bone was generated in the gap; this was called "osteoblastic repair," which means that bone forms faster than bone is resorbed during repair. Therefore, we hope to transform "osteoclastic repair" into "osteoblastic repair" by promoting osteoblast activity while inhibiting osteoclast activity to prevent collapse of the femoral head. Future treatment of femoral head osteonecrosis requires the use of generic drugs, diphosphonate, or Nell-1 to promote osteoblast activity and inhibit osteoclast activity, combined with physical support such as that imparted by impaction grafting. Such combined therapies are appropriate for patients with early-stage osteonecrosis of the femoral head.

Acknowledgements

Competing Interests

The authors have declared that no competing interest exists.

References

1. Gou WL, Lu Q, Wang X, Wang Y, Peng J, Lu SB. Key pathway to prevent the collapse of femoral head in osteonecrosis. European review for medical and pharmacological sciences. 2015; 19: 2766-74.
2. Tripathy SK, Goyal T, Sen RK. Management of femoral head osteonecrosis: Current concepts. Indian journal of orthopaedics. 2015; 49: 28-45.
3. Wright EA, Katz JN, Baron JA, Wright RJ, Malchau H, Mahomed N, et al. Risk factors for revision of primary total hip replacement: results from a national case-control study. Arthritis care & research. 2012; 64: 1879-85.
4. van der Jagt D, Mokete L, Pietrzak J, Zalavras CG, Lieberman JR. Osteonecrosis of the femoral head: evaluation and treatment. The Journal of the American Academy of Orthopaedic Surgeons. 2015; 23: 69-70.
5. Weinstein RS. Glucocorticoid-induced osteoporosis and osteonecrosis. Endocrinology and metabolism clinics of North America. 2012; 41: 595-611.
6. Weinstein RS. Glucocorticoid-induced osteonecrosis. Endocrine. 2012; 41: 183-90.
7. Hao C, Yang S, Xu W, Shen JK, Ye S, Liu X, et al. MiR-708 promotes steroid-induced osteonecrosis of femoral head, suppresses osteogenic differentiation by targeting SMAD3. Sci Rep. 2016; 6: 22599.
8. Okazaki S, Nagoya S, Tateda K, Katada R, Mizuo K, Watanabe S, et al. Weight bearing does not contribute to the development of osteonecrosis of the femoral head. International journal of experimental pathology. 2012; 93: 458-62.
9. Dean MT, Cabanela ME. Transtrochanteric anterior rotational osteotomy for avascular necrosis of the femoral head. Long-term results. The Journal of bone and joint surgery British volume. 1993; 75: 597-601.
10. Yamamoto T, Ikemura S, Iwamoto Y, Sugioka Y. The repair process of osteonecrosis after a transtrochanteric rotational osteotomy. Clinical orthopaedics and related research. 2010; 468: 3186-91.
11. Yamamoto T, Iwasaki K, Iwamoto Y. Transtrochanteric rotational osteotomy for a subchondral insufficiency fracture of the femoral head in young adults. Clinical orthopaedics and related research. 2010; 468: 3181-5.
12. Jones DR. A potential osteoporosis target in the FAS ligand/FAS pathway of osteoblast to osteoclast signaling. Annals of translational medicine. 2015; 3: 189.
13. Jiang Y, Zhang Y, Chen W, Liu C, Li X, Sun D, et al. Achyranthes bidentata extract exerts osteoprotective effects on steroid-induced osteonecrosis of the femoral head in rats by regulating RANKL/RANK/OPG signaling. Journal of translational medicine. 2014; 12: 334.
14. Lunguo Xia, Zhilan Yin, Lixia Mao, Jiaqiang Liu, Xinquan Jiang, Zhiyuan Zhang, et al. Akermanite bioceramics promote osteogenesis, angiogenesis and suppress osteoclastogenesis for osteoporotic bone regeneration. Scientific reports. 2016; 6.
15. Zhou L, Yoon SJ, Jang KY, Moon YJ, Wagle S, Lee KB, et al. COMP-angiopoietin1 potentiates the effects of bone morphogenic protein-2 on ischemic necrosis of the femoral head in rats. PloS one. 2014; 9: e110593.
16. Wang C, Peng J, Lu S. Summary of the various treatments for osteonecrosis of the femoral head by mechanism: A review. Experimental and therapeutic medicine. 2014; 8: 700-6.
17. Ominsky MS, Li X, Asuncion FJ, Barrero M, Warmington KS, Dwyer D, et al. RANKL inhibition with osteoprotegerin increases bone strength by improving cortical and trabecular bone architecture in ovariectomized rats. Journal of bone and mineral research : the official journal of the American Society for Bone and Mineral Research. 2008; 23: 672-82.

18. Li Y, Wang Y, Guo Y, Wang Q, Ouyang Y, Cao Y, et al. OPG and RANKL polymorphisms are associated with alcohol-induced osteonecrosis of the femoral head in the north area of China population in men. Medicine. 2016; 95: e3981.

19. Gori F, Hofbauer LC, Dunstan CR, Spelsberg TC, Khosla S, Riggs BL. The expression of osteoprotegerin and RANK ligand and the support of osteoclast formation by stromal-osteoblast lineage cells is developmentally regulated. Endocrinology. 2000; 141: 4768-76.

20. Cao HJ, Zheng LZ, Wang N, Wang LY, Li Y, Li D, et al. Src blockage by siRNA inhibits VEGF-induced vascular hyperpemeability and osteoclast activity - an in vitro mechanism study for preventing destructive repair of osteonecrosis. Bone. 2015; 74: 58-68.

21. Peskin B, Shupak A, Levin D, Norman D, Jacob Z, Boss JF, et al. Effects of non-weight bearing and hyperbaric oxygen therapy in vascular deprivation-induced osteonecrosis of the rat femoral head. Undersea & hyperbaric medicine : journal of the Undersea and Hyperbaric Medical Society, Inc. 2001; 28: 187-94.

22. Kim HK, Aruwajoye O, Du J, Kamiya N. Local administration of bone morphogenetic protein-2 and bisphosphonate during non-weight-bearing treatment of ischemic osteonecrosis of the femoral head: an experimental investigation in immature pigs. The Journal of bone and joint surgery American volume. 2014; 96: 1515-24.

23. Zhang Y, Yin J, Ding H, Zhang C, Gao YS. Vitamin K2 Ameliorates Damage of Blood Vessels by Glucocorticoid: a Potential Mechanism for Its Protective Effects in Glucocorticoid-induced Osteonecrosis of the Femoral Head in a Rat Model. International journal of biological sciences. 2016; 12: 776-85.

24. Heng-feng Yuan, Von Roemeling Christina, Chang-an Guo, Yi-wei Chu, Rong-hua Liu, Yan Z-q. Involvement of MicroRNA-210 Demethylation in Steroid-associated Osteonecrosis of the Femoral Head. Scientific reports. 2016; 6.

25. Yuan HF, Christina VR, Guo CA, Chu YW, Liu RH, Yan ZQ. Involvement of MicroRNA-210 Demethylation in Steroid-associated Osteonecrosis of the Femoral Head. Sci Rep. 2016; 6: 20046.

26. Wang C, Wang X, Xu XL, Yuan XL, Gou WL, Wang AY, et al. Bone microstructure and regional distribution of osteoblast and osteoclast activity in the osteonecrotic femoral head. PloS one. 2014; 9: e96361.

27. Fan M, Peng J, Wang A, Zhang L, Liu B, Ren Z, et al. Emu model of full-range femoral head osteonecrosis induced focally by an alternating freezing and heating insult. The Journal of international medical research. 2011; 39: 187-98.